Experiments in Fluids 8, 17–24 (1989)

Experiments in Fluids

Instantaneous profiles and turbulence statistics of supersonic free shear layers by Raman excitation plus laser-induced electronic fluorescence (Relief) velocity tagging of oxygen*

R. B. Miles, J. J. Connors, E. C. Markovitz, P. J. Howard, and **G. J. Roth**

Department of Mechanical and Aerospace Engineering, Princeton University, Princeton, NJ 08544, USA

Abstract. A new method of flow tagging based on the vibrational excitation of oxygen is applied to both supersonic and high-speed subsonic air flows to generate instantaneous velocity profiles and turbulence statistics across the free shear layer. By simultaneously tagging two lines, both transverse and streamwise velocity correlations are found. Rayleigh scattering can also be imaged, so this flow diagnostic technique has the capability of instantaneously recording density cross sections and velocity profiles.

1 Introduction

Our understanding of the fundamental properties of turbulence in high-speed flows has been limited by the lack of experimental techniques capable of generating instantaneous multipoint data. In shear layers, turbulent structures and the evolution of these structures play a critical role in heat transfer, drag, and mixing. Previous measurement techniques have relied largely on hot wire probes, laser Doppler velocimetry, and schlieren to infer the properties of turbulent structures. Such fundamental questions as the velocity at which these structures move, the scale of the structures, their form, and the corresponding vorticity fields are unresolved.

This paper outlines a new measurement technique in which lines are instantaneously written into high-speed air and their displacement after a well defined time intervals is recorded. In essence, this technique introduces to the compressible gas community a tool which is similar to the hydrogen bubble flow marking capability which has been so important in water channels (Lu and Smith 1985). Our technique has been applied in both the low-speed and the high-speed flow regimes and requires no seeding since the tracking is done with molecular oxygen. The results presented in this paper show both instantaneous and time-averaged velocities plus turbulence statistics across a Mach 3.6 free shear layer in an axisymmetric free air jet. These results are presented together with subsonic measurements to elucidate the difference between supersonic and subsonic turbulence.

* A version of this paper was presented at the 11th Symposium on Turbulence, University of Missouri-Rolla, Oct. 17–19, 1988

2 Background discussion

The method which is used to tag and follow the flow is a combination of Raman exctiation plus laser-induced electronic fluorescence (Relief) (Miles et al. 1987). It is made possible by the fact that oxygen in its vibrationally excited state has an exceptionally long lifetime (Frey et al. 1972). Consequently, the flow can be tagged by vibrationally exciting oxygen molecules at a specific point or in a line at a given instant in time. At a later instant in time, these molecules are further excited to an electronic state which fluorescens. The fluorescence is recorded on a high-sensitivity camera and the corresponding point displacement or line profile gives a quantitative measure of the velocity and the flow structure. This method differs from velocity measurements which rely on spectral lineshape (Zimmermann and Miles 1980; Kychakoff et al. 1984) where the laser must be tuned across the Doppler-shifted spectral line profile to determine the velocity. Such measurements lead to a time-averaged picture of the velocity field. Here, an instantaneous velocity profile is recorded, so turbulent structure can be seen and both lateral and longitudinal correlations can be made.

Oxygen is a homonuclear diatomic molecule and therefore has no dipole moment. This is responsible for its long vibrational lifetime, but also means that vibrational excitation by the absorption of a single photon is not possible. Consequently, one must use a two-photon process called stimulated Raman scattering to vibrationally excite the molecules. This is done by simultaneously using two lasers which differ in frequency by the vibrational frequency of oxygen. Since stimulated Raman scattering is a nonlinear process, both lasers must be very high intensity to drive a significant number of molecules into the vibrationally excited state. Practically, the intensity is limited by the breakdown threshold of air.

In our experiments, a high-powered Nd:YAG/Nd:YAG pumped dye laser (Quantel Model #YG592) was used to simultaneously generate laser beams at 0.532 μm (green) and 0.580 μm (orange). The pulses were 10 ns in duration and were synchronized in time such that they passed through the

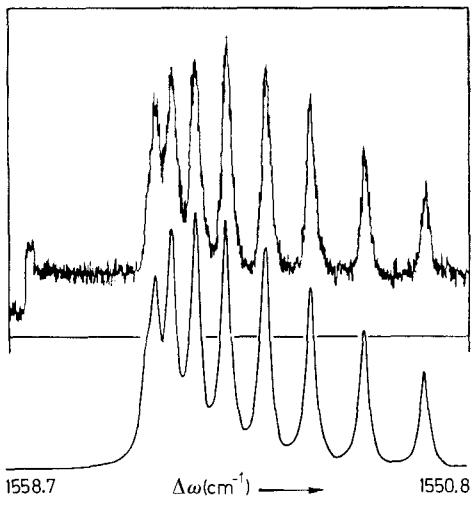

Fig. 1. Rotational structure of the $v'' = 0$ to $v'' = 1$ stimulated Raman transition at 300 K; the upper curve is measured and the lower curve is calculated

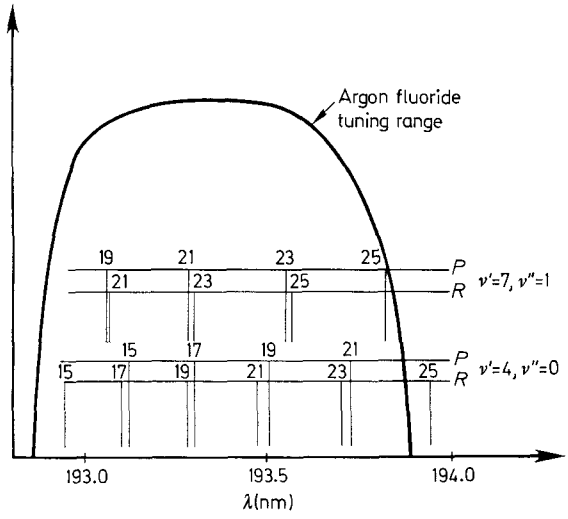

Fig. 2. Overlap of the ArF-laser tuning curve with the transitions from the ground ($v'' = 0$) and vibrationally excited ($v'' = 1$) states of oxygen

tagging volume simultaneously. The maximum energy of the two beams at the test section was 50 mJ and 40 mJ, respectively, and they were focused to a beam diameter of approximately 50 μm measured between the e^{-2} intensity points of the gaussian shaped profiles. This resulted in maximum power densities on the order of 500 GW/cm^2, well in excess of what is required to saturate the transition (Miles et al. 1988), and somewhat higher than the breakdown threshold of air in a static cell. Good flow marking could be seen at considerably lower intensities, but the laser system was operated at the highest intensities possible to optimize the signal-to-noise. The oxygen transitions which are driven with this pair of laser beams correspond to the Q-branch, or those transitions in which the initial and final rotational states are identical. As a consequence, the cooling of the ground state due to the removal of molecules is just offset by the heating of the excited state, so the tagging mechanism leaves the temperature virtually unchanged. The rotational levels of both the ground state and the vibrationally excited state reach thermal equilibrium in a few collisions.

The dye laser is tuned to access the most highly populated rotational state in order to get the largest number of molecules possible into the vibrationally excited state. A plot of the 300 K vibrational excitation versus the frequency difference of the two laser beams is shown in Fig. 1. Since both laser beams are very narrow linewidth (the Nd:YAG laser is injection-locked), the detailed line structure of the rotational states is apparent. For flow tagging, the difference in laser frequencies is selected to correspond to the highest peak in Fig. 1. It is interesting to note that by tuning the dye laser continuously, the rotational populations can be measured which, in turn, give the temperature. Consequently, this technique may also be used to generate a time-averaged temperature profile of the flow field. The bottom curve is the rotational spectrum calculated for 300 K.

The fact that a pair of laser beams must be used to tag the oxygen is a benefit since tagging only occurs where they overlap. In the experiments discussed here, the beams have been made colinear to mark lines in the flow. In general, however, they may be crossed to mark points, crossed at an angle to mark short line segments for vorticity measurements, or multipally crossed to mark two- or three-dimensional grids. Since very little of the laser light is lost in the pumping process, the beams may be reflected back and forth through the flow to simultaneously mark additional lines.

The interrogation step is accomplished with a narrow linewidth ultraviolet ArF excimer laser (Lambda Physik Model #EMG150MSC) which further excites the vibrationally excited molecules up to the $v' = 7$ state in the oxygen Schumann-Runge band. Figure 2 shows the tuning range of the ArF laser and the various lines associated with transitions from the ground and first vibrational state of oxygen which fall within that range. The ArF laser is generally tuned to the P(19) or R(21) lines or the P(23) or R(25) lines of the $v' = 7$, $v'' = 1$ manifold. The P(21) and R(23) lines of that manifold fall on top of absorption lines from the ground state of oxygen and are, consequently, avoided. In fact, transitions from ground state oxygen are not seen because the oxygen in the laser cavity itself and in the air path between the laser and the test cell absorbs those photons. The $v' = 7$ state of the Schumann-Runge band is strongly predissociated so that most of the oxygen molecules excited to that state break apart into oxygen atoms. Only one part in 10^5 of these molecules fluoresce, so the image must be recorded with a high-sensitivity camera. We used a General Electric Model #TN2505 CID camera with a gated ITT F4561

double-microchannel plate intensifier with a maximum gain of 2×10^6. The fluorescence yield is further reduced by the poor Franck-Condon coupling factor between the $v' = 7$ and $v'' = 1$ states, and the fact that only very few of the molecules in the vibrationally excited state lie in the high rotational states which can be accessed by the ArF laser. By choosing other (more complex) ultraviolet lasers, signal enhancements on the order of 1,000 or more can be expected. Nevertheless, interrogated lines are readily visible with the ArF laser, as will be seen later.

The ArF laser generates a large amount of Rayleigh scattering which may be simultaneously imaged to give the density. In our experiments, the ArF laser was loosely focused to a sheet which intersected the flow longitudinally. This sheet was made several hundred microns thick so that the tagged molecules would stay inside the ArF illumination region during the time intervals of interest. If no far UV-blocking filter was used, the Rayleigh scattering was simultaneously collected giving a qualitative picture of the density simultaneous with the line interrogation. When the velocity data was taken, a UV-blocking filter was placed in front of the camera so that only the tagged line was seen.

3 Computer data analysis system

Images were acquired at the 10 Hz repetition rate of the laser systems and were downloaded from the video camera to a frame grabber and then either read directly into the computer or stored on videotape. The videotape provided a permanent record and, in most cases, computer processing was done offline by reading the videotape. A computer program was written which could extract a small rectangular window from each image and rapidly transfer that data into the memory of the SUN 3/160 computer. The window was selected to include that portion of the line of interest. In the cases where two lines were simultaneously marked, the window was expanded to include both lines. After the data was loaded into the computer, the location of the lines was determined by searching for the brightest pixels in each subsequent vertical row of pixels while stepping through each image window from left to right. The search was weighted towards the point located in the previous vertical row of pixels to favor continuity of the line. This allowed multiple lines to be tracked on the same image and eliminated random jumps to bright noise spots far from the tagged line. The center of the line was determined using a weighted sum of the pixels surrounding the brightest pixel. The time delay between marking and interrogation was selected to be short enough to minimize errors due to loops or large bends in the line which lead to double values in the vertical (axial) direction. Only the velocity in the axial direction was measured. (Two- or three-dimensional velocity measurements can be made if points or point grids are written into the flow and tracked in two or three dimensions.)

Following line identification, the image windows were displayed by the computer with the identified line location shown superimposed on the original data. Each individual image was reviewed to be sure that the line or lines identified did, in fact, lie on top of the recorded lines in the image. If not, that particular image window was deleted. When the final set of images was selected, the computer found the average axial velocity profiles and the turbulence intensity. Following that, any point across the velocity profile could be selected and the computer presented a histogram of the velocity values at that point and correlations of the u component of the velocity at that point with the u component of the velocities at the other points across the velocity profile. For the cases where two lines were marked, the computer also generated the correlation of the velocity across the other line with the selected velocity component.

4 Velocity profiles across a supersonic jet

A versatile axisymmetric free jet facility was constructed to provide a test environment for the development of the Relief technique. For the high-speed measurements a sonic orifice was used to generate an underexpanded free jet. The plenum was operated at 150 psia and reached an equilibrium temperature of 250 K. The jet exited into a 1 atm test chamber through a 6.35 mm (0.25″) diameter nozzle. The Reynolds number was approximately 1.2×10^6 based on the exit diameter. An orthographic projection of the test chamber plus the laser beams and camera system is shown in Fig. 3. The tagging beams were focused into the chamber from the left and were reflected back with a mirror so that two lines were simultaneously tagged. The separation between these two lines could be arbitrarily selected. The ArF laser passed through a cylindrical lens and was focused to a sheet of light which entered the chamber from the right. A gated and intensified CID videocamera recorded both the Rayleigh scattering from the air and the laser-induced electronic fluorescence from the tagged oxygen molecules.

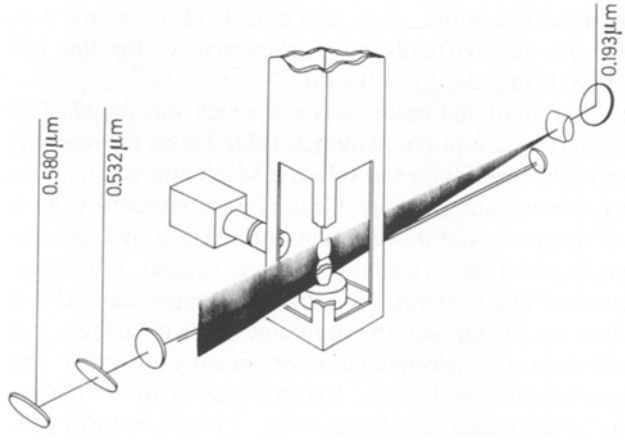

Fig. 3. Orthographic projection of the test region

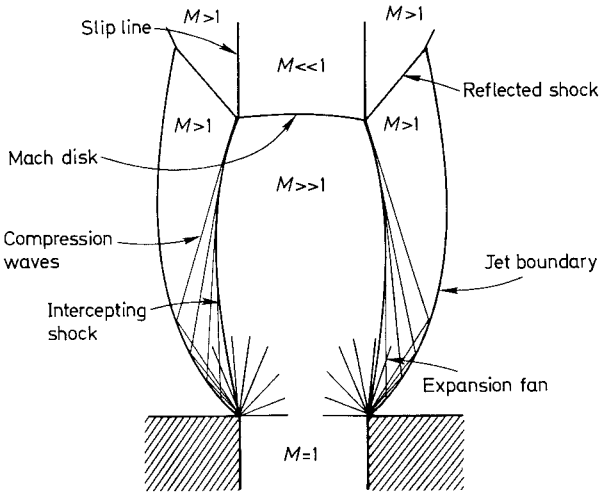

Fig. 4. Structure of an underexpanded sonic jet

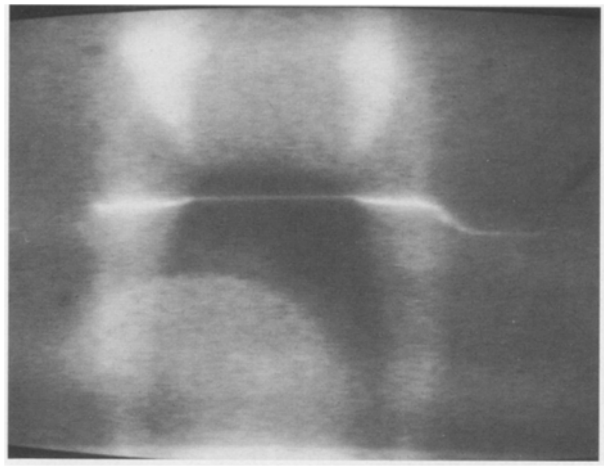

Fig. 5. Cross section of underexpanded jet with a line marked upstream of the Mach disk; the line was straight when marked, so the displacement is a quantitative measure of the velocity profile; Rayleigh scattering is imaged to generate the density (the round feature at the bottom is an artifact due to light scattering)

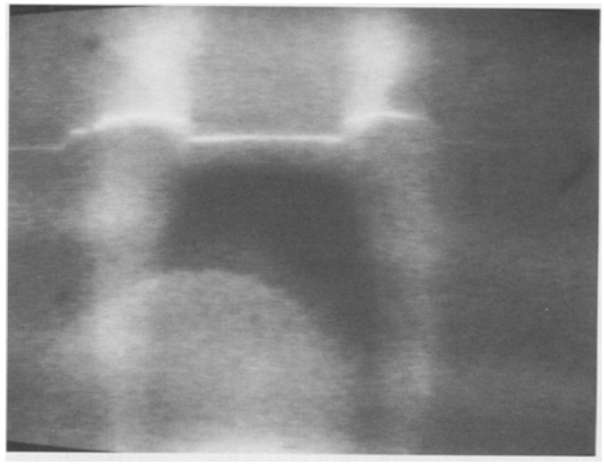

Fig. 6. Cross section of underexpanded jet with a line marked downstream of the Mach disk; the line was straight when marked, so the displacement is a quantitative measure of the velocity profile; Rayleigh scattering is imaged to generate the density (the round feature at the bottom is an artifact due to light scattering)

A diagram of the structure of an underexpanded supersonic free jet is shown in Fig. 4. That structure is echoed in the photographs shown in Fig. 5 and 6 where a line has been marked upstream and downstream of the Mach disk, respectively, in the figures, and the far UV filter has been left off the camera to allow scattering to simultaneously be imaged. In each figure the line was straight when tagged, so the deformation of the line is a quantitative measure of the instantaneous velocity profile. The image was recorded with a single interrogation pulse, approximately 2 μs after the line was tagged.

The Rayleigh scattering gives a qualitative view of the shock structure, the free shear layer, and the density variation. Since the interrogation laser is only on for 10 ns, all of the unsteady phenomenon are frozen. The tagged lines give a quantitative measure of the velocity profile upstream and downstream of the Mach disk. The most notable features are the large discontinuities across the slip lines downstream of the Mach disk. Turbulent structure in the free shear layer can also be seen in both images, and outside of the jet the flow is so slow that virtually no displacement of the line has occured during the 2 μs interval.

A computational model was run which was matched to the operating conditions of our jet. Table 1 gives the computed centerline values for the velocity, Mach number, temperature, density, and pressure. Centerline measurements were made upstream and downstream of the Mach disk as indicated in the Table, yielding measured velocities of 598 ± 20 m/s and 112 ± 20 m/s, respectively. The upstream value is in close agreement with the computed value of 604 m/s, but the downstream measurement is significantly lower than the computed value of 134 m/s. Experimental errors in the velocity measurement are largely due to errors both in calibrating the displacement and measuring the line positions. The camera resolution in the downstream direction is 16.6 microns/pixel, so a 1 pixel error is equivalent to 8 m/s.

We were particularly interested in the characteristics of the turbulence across the free shear layer. Simultaneous two-line flow marking was done with a line separation of 0.76 mm so that velocity correlations in the streamwise direction could be examined. The line positions were approximately 11.2 mm and 11.9 mm from the nozzle exit. The camera and lens were positioned so close-up images across the free shear layer could be observed. The flow was sampled 1 microsecond after tagging and an example of 8 separate line pairs is shown in Fig. 7. The flow is from bottom to top

Table 1. Centerline parameters (calculated) (Dash et al. 1984)

	Location (mm)	Velocity (m/s)	Pressure (pascal)	Temp. (K)	Mach no.	Density g/cc
	0.127	292	5.40×10^5	208	1.01	0.00906
	2.69	433	2.02×10^5	157	1.72	0.00449
	5.23	529	5.95×10^5	111	2.51	0.00187
	7.80	576	2.33×10^4	85	3.13	0.00096
Measurement location	10.3	604	1.12×10^4	68	3.64	0.00057
Mach disk	12.6	621	6.27×10^3	58	4.06	0.00038
Measurement location	13.5	134	1.06×10^5	241	0.43	0.00153

$P_0 = 1.03 \times 10^6$ pascal (150 psia), $T_0 = 250$ K, $P_{\text{ambient}} = 1.01 \times 10^5$ pascal (14.7 psia), exit diameter = 6.35 mm (0.25″)

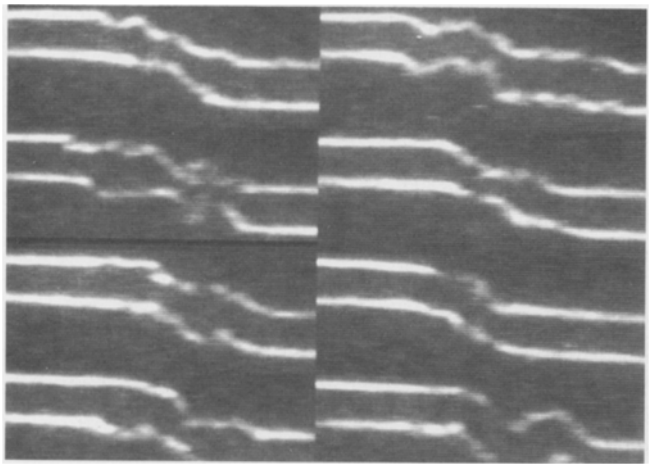

Fig. 7. Tagged line pairs across a supersonic free shear layer

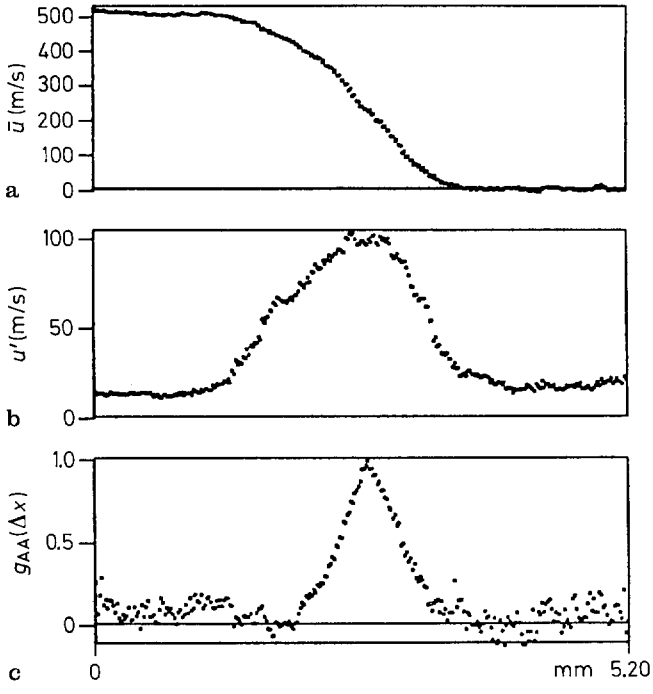

Fig. 8. **a** Average velocity, **b** turbulence intensity, and **c** velocity correlation across a supersonic free shear layer 11.2 mm downstream of the nozzle exit

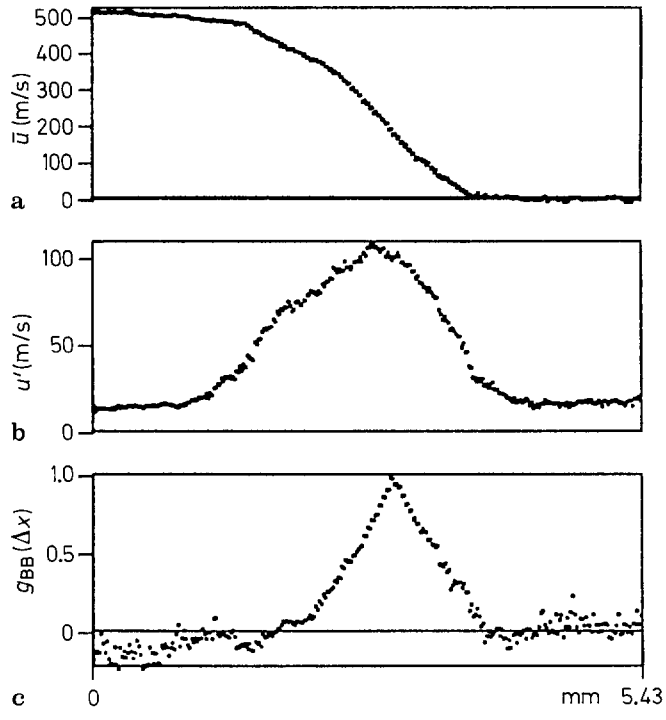

Fig. 9. **a** Average velocity, **b** turbulence intensity, and **c** velocity correlation across a supersonic free shear layer 11.9 mm downstream of the nozzle exit

and the high-speed region is at the left in each image. Approximately 100 such images were used to calculate the average velocity profiles, $U(x)$, and turbulence intensities, $u'(x)$, associated with the two lines. If:

$$u(x) = U(x) - \overline{U(x)} \tag{1}$$

then,

$$u'(x) = \sqrt{\overline{u(x)^2}} \tag{2}$$

These are shown in Figs. 8a and b and 9a and b for the upstream and downstream location respectively.

Lateral velocity correlations can be found by comparing the individual velocity profiles with the average. The two measurement locations are denoted by the subscript A, for

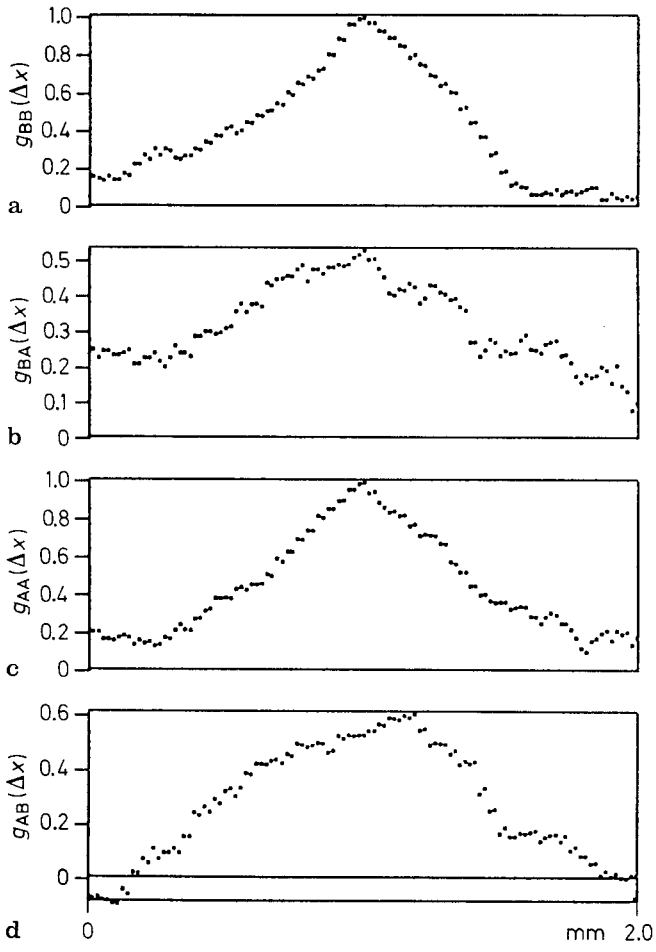

Fig. 10a–d. Expanded view of transverse and streamwise correlations in a supersonic free shear layer; **a** downstream velocity correlation, **b** upstream velocity correlation with the downstream velocity, **c** upstream velocity correlation, **d** downstream correlation with the upstream velocity

the upstream location, and B for the downstream location. The lateral velocity correlation is defined (Hinze 1975):

$$g_{ij}(\Delta x) = \frac{\overline{u_i(x_0)\, u_j(x_0 + \Delta x)}}{u_i'(x_0)\, u_j'(x_0 + \Delta x)} \tag{3}$$

where $i, j = \mathrm{A}$ or B. Figures 8c and 9c show the lateral velocity correlations across the free shear layer at the upstream location, $g_{AA}(\Delta x)$, and at the downstream location, $g_{BB}(\Delta x)$. The correlation point, x_0, is chosen half-way across the shear layer where the mean velocity has fallen to one-half of the maximum. These correlations are a measure of the scale of the turbulence.

The velocities can also be correlated between the two simultaneously tagged lines. Figures 10a through *d* show expanded views of the correlations of the 1/2 velocity point of each line with the velocities in that line and with those in the other line. Figure 10a is an expanded view of Fig. 9c showing the correlation of the velocities across the downstream line with the 1/2 velocity point of that line $[g_{BB}(\Delta x)]$. Figure 10b is the correlation of the velocities across the upstream line with the 1/2 velocity point of the downstream line $[g_{BA}(\Delta x)]$. Figure 10c is an expanded view of Fig. 8c showing the correlation of the velocities across the upstream line with the 1/2 velocity point of that line $[g_{AA}(\Delta x)]$. Figure 10d is the correlation of the velocities across the downstream line with the 1/2 velocity point of the upstream line $[g_{AB}(\Delta x)]$.

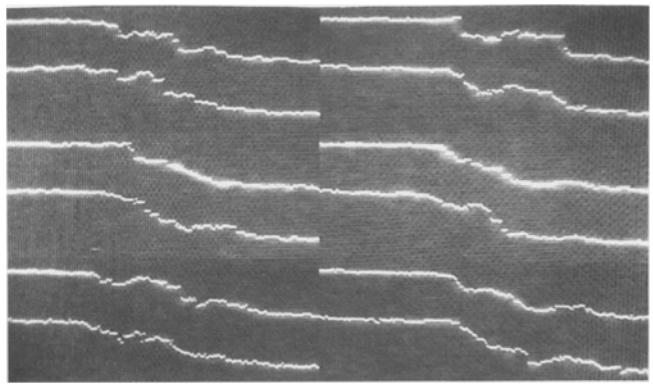

Fig. 11. Tagged line pairs across a high-speed subsonic free shear layer; overlaid bright pixels indicate the computer-identified line position

5 Flow tagging across a low-speed jet

A comparison between subsonic and supersonic flows can be made running the same facility at a lower plenum pressure. In this case the plenum pressure was dropped to 23 psia and the plenum temperature stabilized at 293 K. The tagged lines were separated by 0.74 mm and the downstream line was 12.2 mm from the nozzle exit. The Reynolds number of the jet was approximately 3×10^4 and the time between tagging and interrogation was 2 μs. The centerline velocity was measured to be 273 m/s. A collage of six image windows taken with simultaneous two-line marking across this subsonic jet is shown in Fig. 11. In this case the bright pixels indicating the computer-identified lines are shown superimposed on the data. Once again, the computer calculated the average velocity, the turbulence intensity, and the correlation across the free shear layer as shown in Figs. 12a–c and 13a–c for the upstream and downstream lines, respectively. Correlations done in a manner similar to those in the supersonic flow are shown in Fig. 14a–d.

A comparison of the supersonic and subsonic flows leads to the following observations: (1) The supersonic turbulence intensity appears skewed toward the outer portion of the free shear layer. (2) The supersonic velocity appears to be correlated over a larger fraction of the free shear layer than does the subsonic velocity.

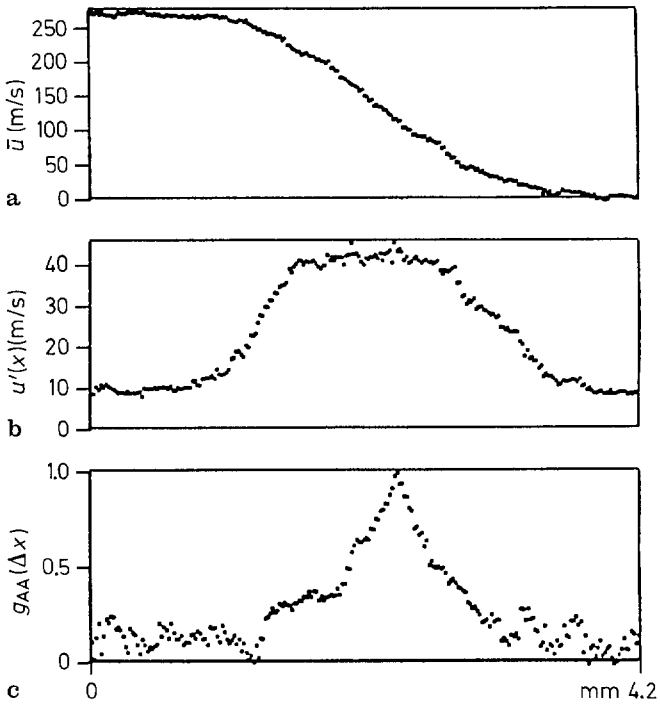

Fig. 12. **a** Average velocity, **b** turbulence intensity, and **c** velocity correlation across a subsonic free shear layer 11.5 mm downstream of the nozzle exit

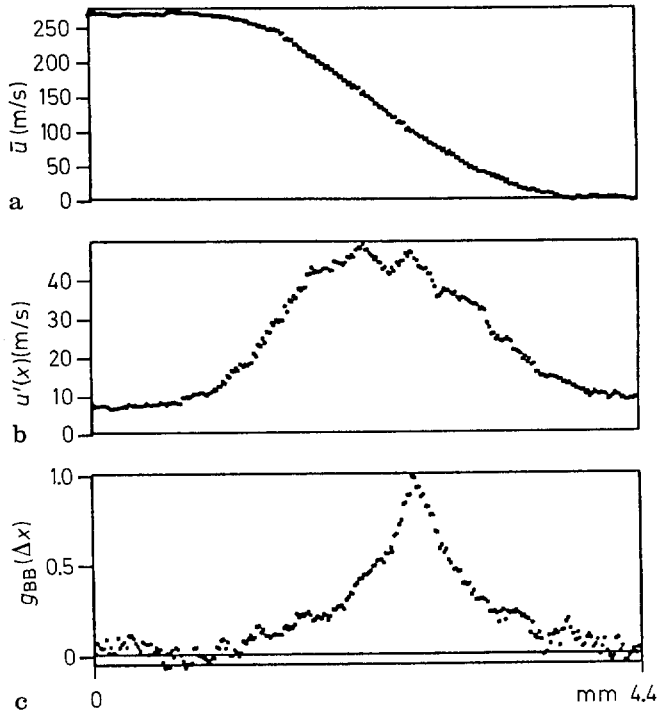

Fig. 13. **a** Average velocity, **b** turbulence intensity, and **c** velocity correlation across a subsonic free shear layer 12.2 mm downstream of the nozzle exit

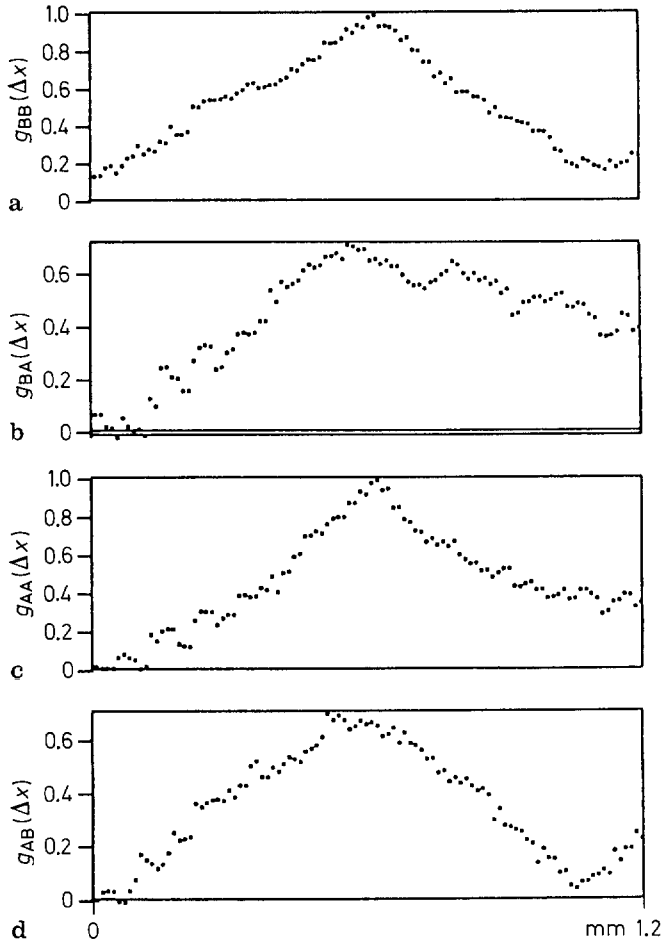

Fig. 14a–d. Expanded view of transverse and streamwise correlations in a subsonic free shear layer; **a** downstream velocity correlation, **b** upstream velocity correlation with the downstream velocity, **c** upstream velocity correlation, **d** downstream correlation with the upstream velocity

Since only on the order of 100 images (limited by the memory of the computer) were sampled to generate the statistics, these observations are tentative.

6 Summary and limitations

The Relief method for tagging both high-speed and low-speed air shows great promise for enhancing our understanding of turbulence. Lines can be instantaneously marked and followed in air flows in much the same manner that hydrogen bubble lines can be tracked in water. In this paper the results of preliminary experiments across the free shear layer of an underexpanded sonic jet have been presented. A comparison with a subsonic jet suggests that there is reduced growth rate of the free shear layer of the supersonic flow. Further experiments using the Relief technique to tag multiple points for three-dimensional velocity field measurements, and small line segments for vorticity measurements will fur-

ther elucidate the characteristics of turbulence both in the high-speed and low-speed regimes. We expect that in the near future the dye laser will be replaced by a high-pressure stimulated Raman cell, and the excimer laser will be replaced by a high-intensity flashlamp. These modifications will significantly simplify the system and reduce its cost.

Due to the fact that vibrationally excited oxygen is being observed, this diagnostic technique is limited to temperatures below approximately 800 K. Above that temperature a significant population of vibrationally excited molecules is generated thermally. The minimum detectable signal level limits the density of air to above about 100 Torr (at 300 K) or 0.12 amagat with the current interrogation set-up. Vibrational relaxation limits the maximum time between tagging and interrogation, Δt. With pure oxygen or air, very slow flows can be observed ($\Delta t > 100$ μs), but when large concentrations of impurities such as water vapor or carbon dioxide are present, vibrational quenching will become a factor, making measurements in slow flows more difficult ($\Delta t < 10$ μs).

Acknowledgements

This work was supported by the U.S. Air Force Office of Scientific Research under Grant Number AFOSR 86-0191. The authors would also like to acknowledge helpful comments from A. Smits and F. Williams.

References

Frey, R.; Lukasik, J.; Ducuing, J. 1972: Tunable Raman excitation and vibrational relaxation in diatomic molecules. Chem. Phys. Lett. 14, 514–517

Hinze, J. O. 1975: Turbulence. 2nd edn. p. 39. New York: McGraw-Hill

Kychakoff, G.; Howe, R. D.; Hanson, R. K. 1984: Quantitative flow visualization technique for measurements in combustion gases. Appl. Opt. 23, 704–712

Lu, L.; Smith, C. 1985: Image processing of hydrogen bubble flow visualization for determination of turbulence statistics and bursting characteristics. Exp. Fluids 3, 349–356

Miles, R.; Cohen, C.; Connors, J.; Howard, P.; Huang, S.; Markovitz, E.; Russell, G. 1987: Velocity measurements by vibrational tagging and fluorescent probing of oxygen. Opt. Lett. 12, 861–863

Miles, R.; Connors, J.; Markovitz, E.; Roth, G. 1988: Coherent anti-Stokes Raman scattering (CARS) and Raman pumping lineshapes in high fields. In: Pulsed single-frequency lasers: technology and applications (eds. Rahn, L.; Bischel, W.) SPIE Vol. 912. Paper #912-26, 184

Zimmermann, M.; Miles, R. B. 1980: Hypersonic-helium-flow-field measurements with the resonant Doppler velocimeter. App. Phys. Lett. 37, 885–887

Received April 25, 1989